BULLETIN OF THE POLISH ACADEMY OF SCIENCES
TECHNICAL SCIENCES, Vol. 71(2), 2023, Article number: e145566
DOI: 10.24425/bpasts.2023.145566

Simulation of a cylindrical glass dome negative impact on a 360° field of view 2D laser scanner performance and a method for correction

Jacek WOJTANOWSKI*

Institute of Optoelectronics, Military University of Technology, ul. gen. Sylwestra Kaliskiego 2, 00-908 Warsaw, Poland

Abstract. Although laser scanning ideas and hardware solutions are well-known to experts in the field, there is still a large area for optimization. Especially, if long-range and high-resolution scanning is considered, the smallest defects in optical quality should be perfected. On the other hand, the simplicity, reliability, and finally the cost of the solution plays an important role, too. In this paper, a very simple but efficient method of optical correction is presented. It is dedicated to laser scanners operating from inside cylindrical glass domes. Such covers normally introduce aberrations into both the laser beam and receiving optics. If these effects are uncorrected, the laser scanner performance is degraded both in terms of angular resolution and maximum range of operation. It may not be critical for short-range scanning applications; however, if more challenging concepts are considered, this issue becomes crucial. The proposed method does not require sophisticated optical solutions based on aspheric or freeform components, which are frequently used for similar purposes in imaging-through-dome correction but is based on a simple cylindrical refractive correction plate.

Key words: laser scanner; laser range finder; laser terrestrial scanning.

1. INTRODUCTION

Laser scanning or terrestrial laser scanning (TLS) is a well-known technique applied in countless applications. Initially, being exclusively the domain of single high-technology military and space solutions, nowadays its availability is used widely in many areas, ranging from science to industry and also covering art and medicine [1–9]. There is a constantly growing number of new concepts and ideas for the implementation of these technologies in a variety of novel configurations in many disciplines [10–20]. Such popularity of laser scanning results from the fact that it provides three-dimensional information about the surrounding reality, something which is not possible for classical (2D) imaging [21–25].

Most laser scanners consist of at least one laser range-finding [26] module (LRF) and mechanical component(s) responsible for redirecting its angular orientation. There is a variety of solutions concerning both LRF and scanning mechanics. Depending on whether the scanned angular domain is one or two-dimensional, one or two-mirror systems can be applied. Let us consider a 2D case (measured: angle, distance). The easiest method, one hypothetically can imagine is to place LRF on a rotating stage (Fig. 1). It is a purely mechanical solution, in most cases probably not recommended, due to the complications resulting from the rotation of the whole LRF module which, after all, must be powered, controlled and must transmit data.

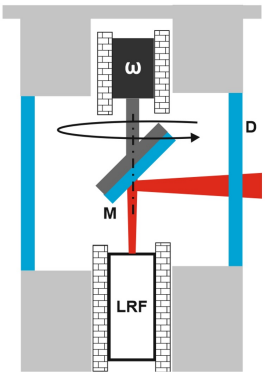

Fig. 1. The idea of a 2D scanning method realized by simple rotation of a laser range finding module (LRF)

Another potentially more useful option is to place a stationary LRF module, in front of a rotating mirror (Fig. 2). Such a solution has a much greater application potential. The only rotating element is a lightweight optical component, which is completely passive – it does not require any electronics connection installation. Mechanically, such a configuration has a lower moment of inertia, if compared to the previous one (Fig. 1) which is an additional asset.

Another important factor for the operation of most scanners results from the need to avoid solutions, where moving parts remain unsecured or even protrude outwards. In such circumstances, they could be accidentally touched by a user, which would pose a grave danger. Additionally, especially for those scanners, which operate in terrain, such "open" configurations

*e-mail: jacek.wojtanowski@wat.edu.pl

Manuscript submitted 2023-02-06, revised 2023-02-06, initially accepted for publication 2023-03-07, published in June 2023.

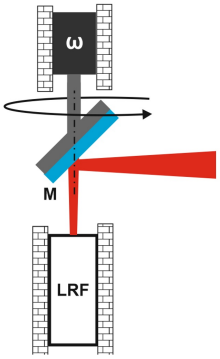

Fig. 2. The alternative idea of a 2D scanning method realized by rotation of a tilted mirror M (LRF fixed)

would expose optics and mechanics to dust, dirt, and humidity. Therefore, the aim is always to obtain a solution which encompasses both rangefinder and rotating mechanical/optical parts. This challenge corresponds to the need for some kind of dome, made of transparent (at least at LRF wavelength) material such as glass or plastic (Fig. 3).

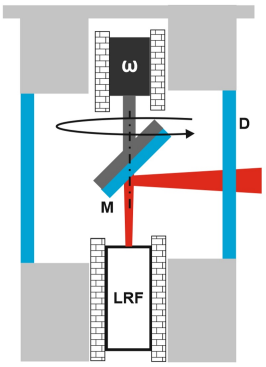

Fig. 3. Schematic representation of a 2D scanner operating from inside a glass dome (D) – cross-section view

Due to the rotational symmetry of typical one-angle laser scanner solutions, the most natural shape of a dome seems to be a cylindrical glass (plastic) pipe. One has to consider, however, that from an optical point of view, it corresponds to a toroidal lens, which might have an impact on LRF performance. Depending on the used glass refractive index, cylinder radii of curvature, and thickness, such impact can be crucial or negligible. Considering the lens-makers equation [27], one can obtain the lens focal length f, if refractive index n, radii of curvature R_1, R_2, and lens thickness t are known

$$\frac{1}{f} = (n-1)\left(\frac{1}{R_1} - \frac{1}{R_2} + \frac{(n-1)t}{nR_1R_2}\right). \tag{1}$$

This equation allows us to conclude that a piece of cylindrical dome acts like a weak cylindrical negative lens, at least at its paraxial region. For example, regarding a 100 mm diameter dome, made of 3 mm thick glass ($n = 1.5$) one arrives at a –9.7 m focal length. Figure 4 depicts in an exaggerated way

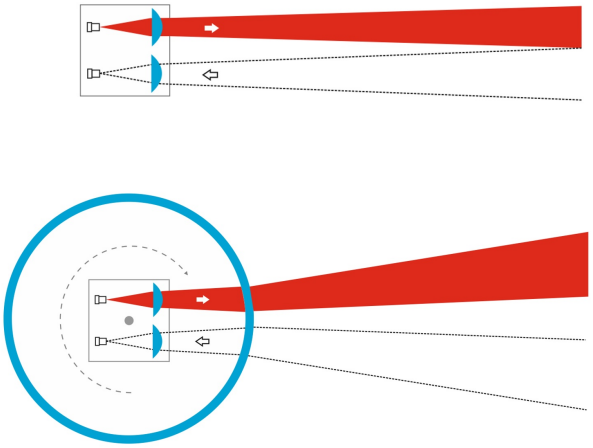

Fig. 4. The idea of cylindrical dome application and its impact on LRF laser beam and LRF detector field of view (upper plot: pure LRF, lower plot: LRF operating from inside a dome)

how a cylindrical dome can distort both the laser beam and the detector field of view of the scanner LRF module.

It can be clearly seen that the originally parallel optical axes of the transmitter and receiver are skewed. Additionally, due to the wavefront distortion, both the laser beam and detector field of view (which can be also treated like a beam of rays) change their divergences. Apart from these effects, it is worth noting that a certain amount of spherical aberration can be induced, which also strongly impacts the performance of any range finder [28].

Again, taking as an example a 100 mm radius of curvature and a 3 mm thick dome made of glass ($n = 1.5$), its effect on a collimated beam of light has been simulated in Optic Studio (configuration detailed in Fig. 5).

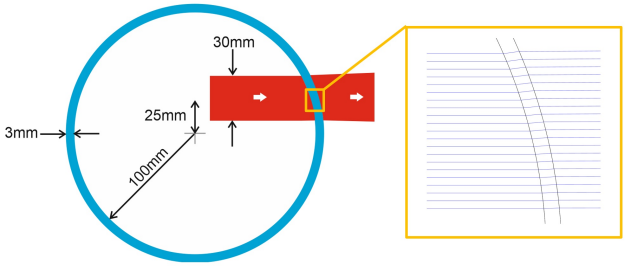

Fig. 5. An example – illustration of cylindrical glass dome impact on collimated rays of light resulting from refraction

It can be observed that in this specific case (whose order of size is quite representative for many potential automotive and military scanning solutions), the glass dome induces ~8 waves (peak-to-valley, PV) of wavefront error (for $\lambda = 0.9\ \mu$m) resulting mainly from spherical aberration and is associated also with a slight wavefront tilt (Fig. 6). These factors correspond to the output beam:

- divergence of 1.8 mrad (root mean square, RMS) or 4 mrad (total),
- tilt of 2.6 mrad.

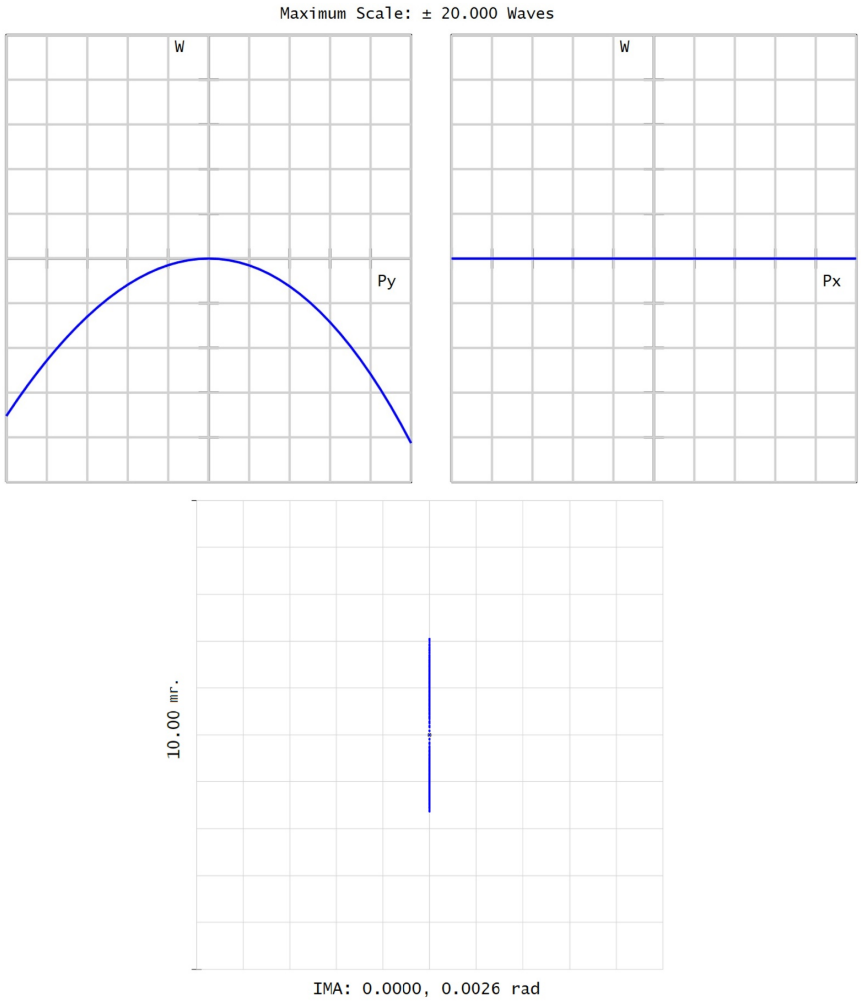

Fig. 6. Results of optical performance analysis of the discussed case study (upper plots: wavefront error in the tangential and sagittal plane, lower plot: far-field angular ray distribution)

Considering most long and medium-range applications, such degradation of optical performance is not acceptable. For this reason, one can find different solutions, which at the cost of certain design compromises, facilitate avoiding the optical issues associated with cylindrical dome application. Most of such concepts rely either on rotating the whole optomechanics or on optical plane glass windows, which are easily available up to $\lambda/10$ flatness (Fig. 7).

Such plane-parallel plates have negligible impact on LRF parameters, although to construct a dome from such components, one has to consider the increased size, manufacturing complexity/price, and potential angular variations of LRF range performance corresponding to the locations of plate connections.

Some manufacturers do use cylindrical glass domes; however, such solutions are either devoted to short-range/low-resolution applications or are costly. In the former cases, the destructive dome impact can be accepted and considered in evaluating the final parameters of the scanner. In the latter cases, on the other hand, advanced optical methods for dome correction can be applied, including freeform mirrors and lens implementation.

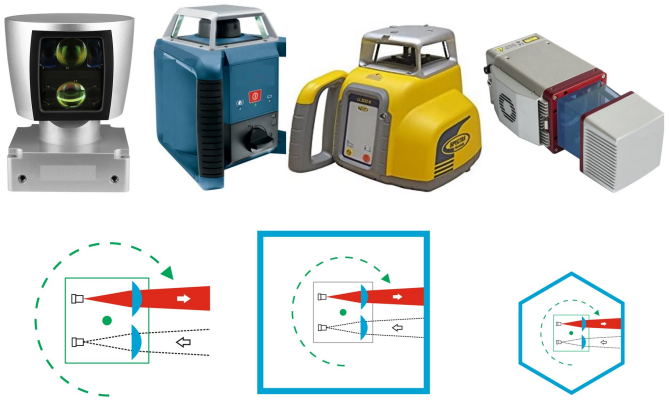

Fig. 7. The examples of common dome constructions based on flat plates in order to avoid the effects induced by a cylindrical dome (upper row: commercially available solutions, lower row: basic ideas)

For these reasons, it seemed to be reasonable to find the point in the middle and to consider the use of a cylindrical dome but with a simple correction strategy. This work aimed to show the

adequate optical correction method that can easily eliminate the discussed undesirable effects on LRF module performance used in a one-angle scanning laser scanner. The method is based on correcting lens application in front of LRF optics.

2. QUANTITATIVE ANALYSIS OF LRF GEOMETRICAL OVERLAP FACTOR DEGRADATION DUE TO CYLINDRICAL DOME APPLICATION

There is a variety of well-recognized criteria for optical system performance, like modulation transfer function (MTF), resolution, point spread function geometry, aberration coefficients, wavefront coefficients, etc. However, in the problem discussed in this paper, such criteria applied to a cylindrical dome would be inconclusive as to the degree of deterioration in the performance of the LRF. For this reason, a new metric directly linked to the LRF range efficiency, is proposed. Let us consider a standard range-finder equation [29]

$$P(z) = P_L \frac{A_0}{z^2} \xi(z) \rho e^{-2\gamma(z)z}, \tag{2}$$

where $P(z)$ represents the optical power of the echo signal as a function of range z, P_L – the power of the laser, A_0 – collecting optics aperture area, $\xi(z)$ – geometrical form (overlap) factor, ρ – target reflectance, $\gamma(z)$ – atmospheric extinction coefficient. The effects of dome impact can be included in geometrical form factor $\xi(z)$, a similar approach to the one presented in [30]. For any LRF configuration, this range-resolved function shows how effectively the detector can capture light from the laser footprint on a target, due to purely geometrical reasons associated with the fact that the detector field of view and laser beam do not coincide or do not completely overlap. This effect is particularly crucial for small detection ranges. In normal conditions and properly designed LRF optics, $\xi(z)$ is a function monotonically increasing from zero (for $z = 0$ m) to one (for $z \Rightarrow z^*$, $z > 0$ m). It is worth noting that this function does not consider the reflectance properties of the target and atmospheric extinction. For the sake of this analysis, the atmospheric impact can be neglected (relatively short ranges). Thus, equation (2) can be transformed to the following form

$$P(z) = \frac{K}{z^2} \xi(z), \tag{3}$$

where K is a range-independent constant parameter that considers lidar hardware and target properties.

The effects of the cylindrical dome, as mentioned in Introduction, lead to a skewing of both the LRF laser beam and detector field of view, which severely impacts the effectiveness of geometrical coupling between both. For this reason, in this paper, the concept of geometrical form factor is expanded to also include the effects of optical aberrations induced by cylindrical domes.

The $\xi(z)$ function can be calculated in the simplest cases by symbolic formulas; however, in the general case of non-symmetric aberrated optics and arbitrary aperture shapes, the most reasonable approach seems to be numerical, preferably based on the application of commercially available optical software. Namely, let us consider the LRF module to be based on the transmitter (LRF_T) and receiver (LRF_R). Now, for the sake of $\xi(z)$ calculation, we will treat LRF_R as a "second" transmitter – the detector emits rays that are collimated by the LRF_R lens, creating a hypothetical beam of light. Then, $\xi(z)$ is calculated from the following formula

$$\xi(z) = \frac{P_\cap(z)}{P_{\text{LRF\_T}}}, \tag{4}$$

where $P_\cap$ corresponds to the optical power integrated over the common area of the LRF_T beam and LRF_R field of view, $P_{\text{LRF\_T}} = P_L$. $P_\cap$ can be found by integrating the irradiance $S_{\text{LRF\_T}}$ over the area $A^*(z)$ where $S_{\text{LRF\_T}}$ and $S_{\text{LRF\_R}}$ spatially overlap

$$P_\cap(z) = \iint\limits_{(x,y)\in A^*(z)} S_{\text{LRF\_T}}(x,y)\,\mathrm{d}x\,\mathrm{d}y, \tag{5}$$

where $A^*(z)$ can be calculated by the application of the following logical filter

$$\begin{aligned} A^* = \{(x,y):\ & [S_{\text{LRF\_T}}(x,y) + S_{\text{LRF\_R}}(x,y) \\ & \neq S_{\text{LRF\_T}}(x,y) \cap S_{\text{LRF\_T}}(x,y) + S_{\text{LRF\_R}}(x,y) \\ & \neq\ S_{\text{LRF\_R}}(x,y)]\}. \end{aligned} \tag{6}$$

In other words, to find the area $A^*(z')$, the potential target plane (x,y,z') is searched for those points (x,y) where the irradiance resulting from individual contributions of LRF_T and LRF_R examined separately, changes in case of simultaneous illumination from both LRF_T and LRF-R. Such an approach must correspond not only to the spatial extent of overlap but also to the distribution of optical coupling efficiency between LRF_T and LRF_R in (x,y) plane for any z. Additionally, in contrast to the existing analytical formulas, the presented method takes into account the real geometry of detecting and emitting semiconductor structures, transmitting and receiving apertures shapes, and finally also the aberrations of collimating and collecting optics.

To present the practical application of this approach, let us continue with the specific Case Study detailed in Fig. 8. The configuration corresponds to the common semiconductor laser-based setup:

- transmitter aperture takes the rectangular shape due to the asymmetric divergence angles of a native laser beam (fast and slow axes),
- emitting structure of the semiconductor laser is also represented by the rectangle due to the stacked stripe emitters system used in high peak power pulsed laser.

This case will also become the core of this study in later analysis, where the impact of the dome is examined and also the effectiveness of the proposed correction method is verified.

The discussed setup was implemented in a non-sequential mode of Optic Studio. In order to separate the effects induced by a toroidal dome in later steps, the roles of collimating and collecting optics played perfect (paraxial) lenses. The purpose of this implementation was to obtain the spatial distributions of

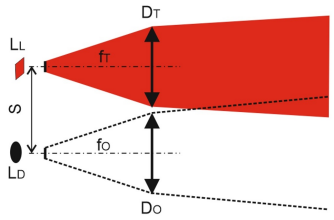

Parameter	Value
Emitting structure shape	Rectangular
Emitting structure size, LL_x x LL_y	75 x 15 μm
Transmitter lens focal length, f_T	50 mm
Transmitter aperture shape	Circular
Transmitter aperture diameter, D_T	40 mm
Transmitter-Receiver separation, S	42 mm
Detecting structure shape	Round
Detecting structure size, L_D	300 μm
Receiver lens focal length, f_0	50 mm
Receiver aperture shape	Circular
Receiver aperture diameter, D_0	40 mm

Fig. 8. Case Study – basic configuration of LRF without a dome

$S_{LRF\_T}(x,y)$ and $S_{LRF\_R}(x,y)$ for the selection of various distances z. The results are shown in Fig. 9.

The obtained distributions (Fig. 9) were then imported from Optic Studio to Matlab and used in the proposed method to calculate the geometrical form factor, which for this dome-less

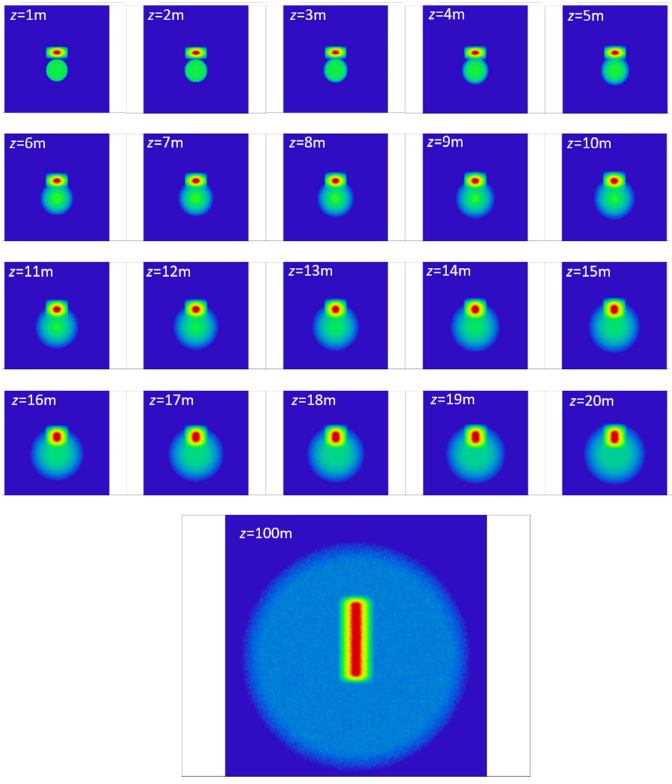

Fig. 9. Results of numerical modelling (geometrical ray-tracing) of $S_{LRF\_T}(x,y)$ and $S_{LRF\_R}(x,y)$ distributions at the selected distances $z =$ 1, 2, 3, 4, 5, 6, 7, 8, 9, 10, 11, 12, 13, 14, 15, 16, 17, 18, 19, 20, 100 m for the considered example of LRF dome-less operation

setup will be designated as $\xi_{LRF}(z)$. In the next step, the modelled setup was changed by adding a glass dome to the LRF (Fig. 10).

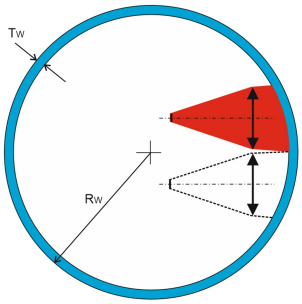

Fig. 10. Configuration of LRF operating from inside the dome (Case Study parameters: $R_w = 75$ mm, $T_w = 3$ mm, $n = 1.5$)

The corresponding distributions of $S_{LRF\_T}(x,y)$ and $S_{LRF\_R}(x,y)$ are shown in Fig. 11. One can clearly notice the impact of the dome – both laser beam and detector field of view footprints are stretched in the direction determined by dome curvature and also their centres do not overlap.

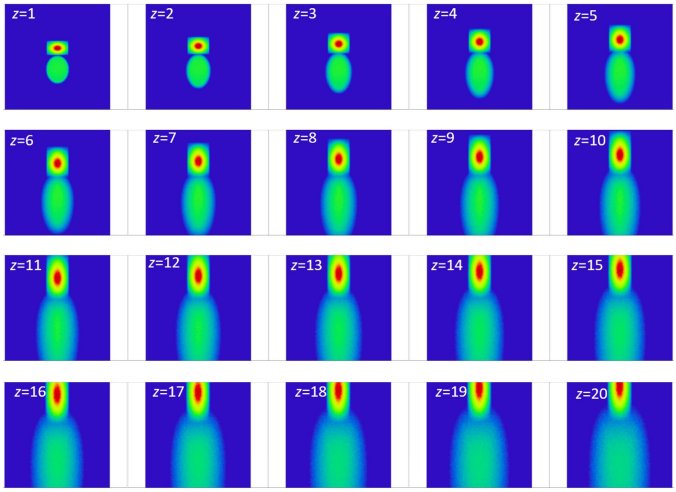

Fig. 11. Results of numerical modelling (geometrical ray-tracing) of $S_{LRF\_T}(x,y)$ and $S_{LRF\_R}(x,y)$ distributions at the selected distances $z =$ 1, 2, 3, 4, 5, 6, 7, 8, 9, 10, 11, 12, 13, 14, 15, 16, 17, 18, 19, 20 m for the considered example of LRF operating from inside the glass dome

Apart from this effect, it can also be concluded that even for larger distances z, $S_{LRF\_T}(x,y)$ and $S_{LRF\_R}(x,y)$ do not completely overlap. It corresponds to the situation where the geometrical form factor does not reach the value of one. In such a case, the LRF detector cannot "fully see" the LRF laser footprint on a target. It leads to the degradation of the overall photon budget (a lot of optical power is lost) and the reduction of the maximum usable operational range.

Similarly, the distributions presented in Fig. 11 were imported and implemented in the proposed algorithm. It facilitated the calculation of the geometrical form factor, which for the discussed setup (LRF+dome) will be designated as $\xi_{LRF+D}(z)$.

The obtained results in terms of geometrical form factor and also optical echo power, for both setups, are presented in Fig. 12. It is evident how significantly the dome affects the performance of the LRF and how severely the maximum usable range is reduced.

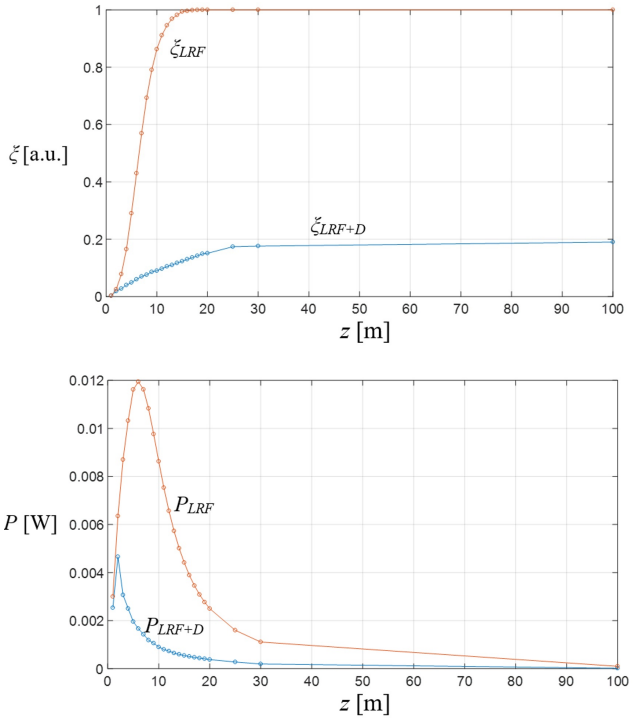

Fig. 12. Upper plot shows superimposed geometrical form factor functions of the case study ($\xi_{\mathrm{LRF}}(z)$ for the pure LRF module and $\xi_{\mathrm{LRF+D}}(z)$ for the LRF covered by a cylindrical dome). The lower plot presents the corresponding range of resolved optical echo power functions for both cases

This allowed us to prove quantitatively that the configuration where an LRF is covered by a cylindrical glass dome is not acceptable and requires either some optical correction or a complete change of covering method. The former approach is the objective of the presented paper.

3. PROPOSED CORRECTION METHOD

In order to reduce the impact of the dome on LRF performance, an optical method of correction was developed. It is based on geometrical optics rules and energy mapping methodology. The main numerical target of the proposed scheme is to retrieve the satisfactory distribution of $\xi_{\mathrm{LRF+D}}(z)$, which should be as close as possible to the original geometrical form factor $\xi_{\mathrm{LRF}}z)$. Below, the method is described in more detail.

First of all, let the distributions $S_{\mathrm{LRF\_T}}(x_i, y_j)$ and $S_{\mathrm{LRF\_R}}(x_i, y_j)$ for the selection of discreet distances z_k be designated as $S^{ijk}_{\mathrm{LRF\_T}}$ and $S^{ijk}_{\mathrm{LRF\_R}}$. It is worth noting that the indices i, j, k correspond to the discretization of x, y, and z dimensions respectively. Then, let us introduce range-resolved vector functions $\rho^k_{\mathrm{LRF\_T}}$ and $\rho^k_{\mathrm{LRF\_R}}$ which correspond to the "energetic centres of gravity" of $S^{ijk}_{\mathrm{LRF\_T}}$ and $S^{ijk}_{\mathrm{LRF\_R}}$ in (i, j) domain for the respective k values. These functions are defined as follows

$$\boldsymbol{\rho}^k_{\mathrm{LRF\_T}} = \left(\frac{\sum_i \left[\sum_j S^{ij}_{\mathrm{LRF\_T}} \right] x_i}{\sum_{i,j} S^{ij}_{\mathrm{LRF\_T}}}, \frac{\sum_j \left[\sum_i S^{ij}_{\mathrm{LRF\_T}} \right] y_j}{\sum_{i,j} S^{ij}_{\mathrm{LRF\_T}}} \right), \quad (7)$$

$$\boldsymbol{\rho}^k_{\mathrm{LRF\_R}} = \left(\frac{\sum_i \left[\sum_j S^{ij}_{\mathrm{LRF\_R}} \right] x_i}{\sum_{i,j} S^{ij}_{\mathrm{LRF\_R}}}, \frac{\sum_j \left[\sum_i S^{ij}_{\mathrm{LRF\_R}} \right] y_j}{\sum_{i,j} S^{ij}_{\mathrm{LRF\_R}}} \right). \quad (8)$$

They allow us to obtain the range-resolved trajectory of energetic centres of gravity associated with the LRF laser beam and LRF detector field of view. In the case of pure LRF operation, both trajectories should be represented by parallel lines. On the other hand, if a dome is introduced, these trajectories represent the net effect of non-parallelism introduced and the stretching of distributions due to any aberrations induced by the dome. For the discussed case study, results are presented in Fig. 13, showing the calculated trajectories of energetic centres of gravity both for "pure LRF" and "LRF+dome" configuration, which were denoted as $\rho^k_{\mathrm{LRF\_T(R)}}$ and $\rho^k_{\mathrm{LRF\_T(R)\_D}}$.

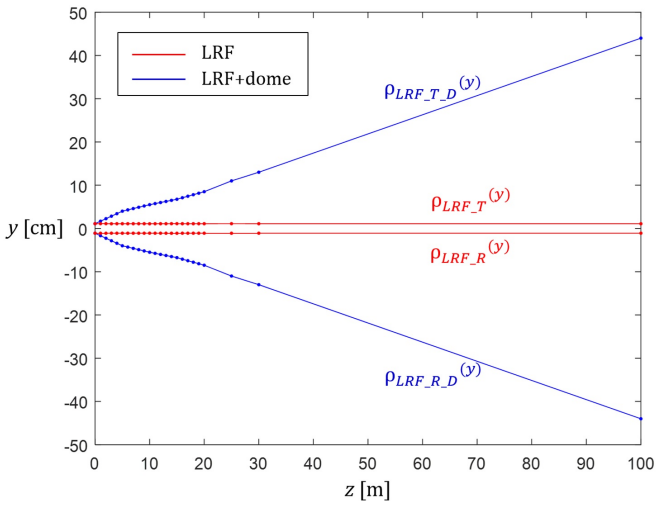

Fig. 13. Numerically calculated centres of gravity (y, z) coordinates for both transmitter and receiver beams in case of undisturbed LRF (red colour) and LRF operating from inside the glass dome (blue colour)

In the next step $\rho^k_{\mathrm{LRF\_T(R)\_D}}$ functions were used to calculate their closest linear representations, designated as $y_{\mathrm{LRF\_T\_D}}(z) = a_{\mathrm{LRF\_T\_D}} \cdot z + b_{\mathrm{LRF\_T\_D}}$ and $y_{\mathrm{LRF\_R\_D}}(z) = a_{\mathrm{LRF\_R\_D}} \cdot z + b_{\mathrm{LRF\_R\_D}}$. The coefficients a_{LRF} and b_{LRF} were easily calculated by the application of the traditional least squares method. The obtained straight lines were then thought of as virtual chief rays of both beams (laser beam and detector "beam"). Due to the symmetry of these rays with respect to $y = 0$ axis, the resulting coefficients $a_{\mathrm{LRF\_T\_D}} \approx a_{\mathrm{LRF\_R\_D}} \equiv a_{\mathrm{LRF\_D}}$, $|b_{\mathrm{LRF\_T\_D}}| =$

$|b_{\text{LRF\_R\_D}}| \equiv b_{\text{LRF\_D}}$. Finally, based on principles of geometrical optics ray tracing [31], a radius of curvature of the refractive spherical surface required to recollimate these rays can be determined (Fig. 14).

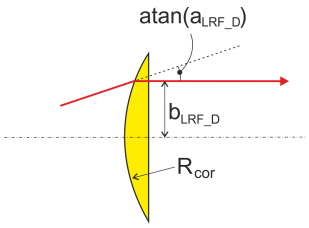

Fig. 14. Raytracing idea of the correcting cylindrical lens

The corresponding formula for the correcting lens radius of curvature is as follows

$$R_{\text{cor}} = \frac{n \cdot b_{\text{LRF\_D}}}{a_{\text{LRF\_D}}}, \tag{9}$$

where n is the refractive index of lens glass at the laser wavelength. Concerning the discussed case study, it corresponds to $R_{\text{cor}} = 2567.5$ mm. Additionally, considering the separation (42 mm) and diameters (40 mm) of the transmitter and receiver apertures, the minimum physical size (diameter) of the correcting cylindrical lens could be determined as 90 mm. It was decided to assume 8 mm of thickness to make the fabrication of the lens feasible. Such a lens (made of N-BK7 optical glass) was implemented in Optic Studio. It was inserted between LRF and the dome (Fig. 15).

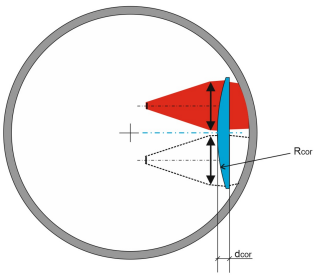

Fig. 15. Correcting cylindrical lens implementation idea (in the discussed case study: $R_{\text{cor}} = 2567.5$ mm, $d_{\text{cor}} = 8$ mm)

The results of numerical modelling in Optic Studio are presented in Fig. 16. It can be clearly seen that the idea of correction worked properly. If compared to the original situation presented in Fig. 9 (LRF without dome), there are differences in irradiance distributions. It corresponds to the aberrations introduced by the composition of correcting lens and a dome. Nevertheless, the main purpose of the correction seemed to be achieved – both beams were forced to have a common overlap.

The obtained irradiance distributions were again used to calculate the corresponding geometrical form factor, which for the discussed setup (LRF+dome+correction) will be designated as $\xi_{\text{LRF+D+COR}}(z)$. It is presented in Fig. 17.

Comparing $\xi_{\text{LRF+D+COR}}(z)$ and $\xi_{\text{LRF}}(z)$ presented in Fig. 12, one can see a very close similarity between both. In other words, the numerical simulation proved that the correction enabled the recovery of the original geometrical form factor of LRF, despite the dome impact.

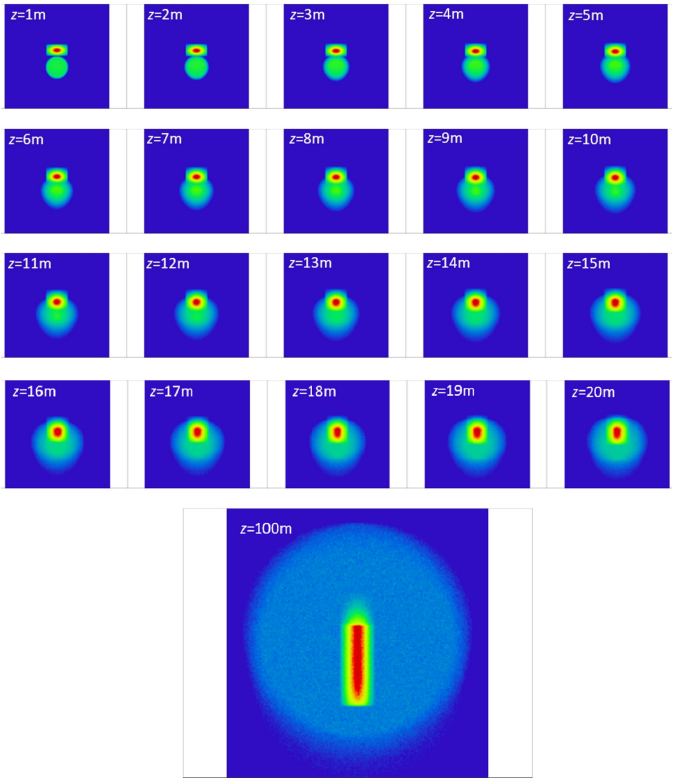

Fig. 16. Results of numerical modelling (geometrical ray-tracing) of $S_{\text{LRF\_T}}(x,y)$ and $S_{\text{LRF\_R}}(x,y)$ distributions at the selected distances $z =$ 1, 2, 3, 4, 5, 6, 7, 8, 9, 10, 11, 12, 13, 14, 15, 16, 17, 18, 19, 20, 100 m for the considered example of LRF operating from inside the glass dome, however with the correction lens implemented

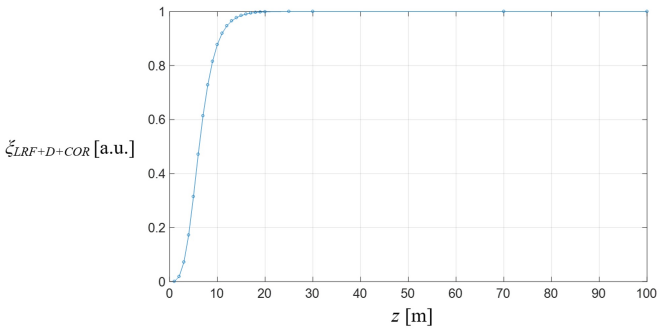

Fig. 17. Results of numerical modelling – geometrical form factor for the LRF operating from inside the dome, with the correcting lens implemented

4. EXPERIMENTAL VALIDATION

In order to practically verify the effectiveness of the proposed method, the experimental setup was prepared. The procedure aimed to measure $P(z)$ before and after the implementation of the proposed correcting lens. Such measurements were

planned in order to determine the corresponding overlap factors: $\xi_{\mathrm{LRF}}(z)$, $\xi_{\mathrm{LRF+D}}(z)$, and $\xi_{\mathrm{LRF+D+COR}}(z)$, and finally to assess the results of the correction. What is important, it was not necessary to build a complete LRF module, since inherent range-finding capability was not needed for this experiment. Thus, the system could be assembled easily, mainly from the components available in our lab (Fig. 18).

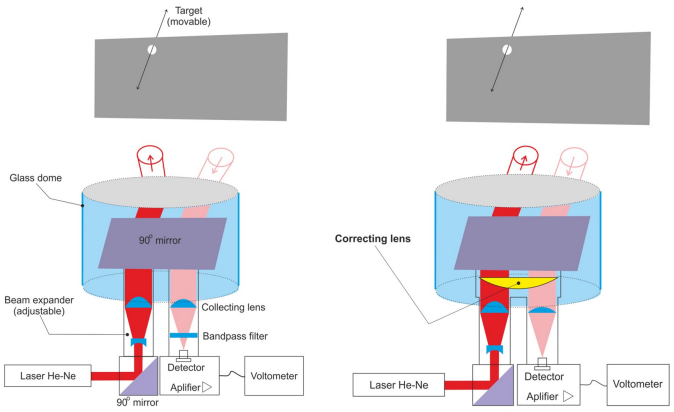

Fig. 18. Diagram of the experimental setup (left without correction – determination of $\xi_{\mathrm{LRF+D}}(z)$, right: with the correcting lens – determination of $\xi_{\mathrm{LRF+D+COR}}(z)$)

This system design aimed to obtain the same geometrical parameters as in the case study discussed in this paper (see table in Fig. 8). First of all, the He-Ne laser ($\lambda = 633$ nm) was used as the source of radiation. In order to control the output beam size and divergence, the adjustable beam expander was implemented. It was based on Galilean configuration, so one negative and one positive lens was used. Both lenses were COTS plano-spherical components. The receiving path was based on a PIN photodiode which cooperated with a plano-convex collecting lens and 633 nm CWL bandpass filter in order to minimize ambient light-related interferences. In order to measure the signal level, an oscilloscope was used as a voltmeter. Additionally, 90° mirrors were used to obtain the geometry similar to the actual laser scanning systems. Finally, the glass dome was positioned in such a way that both the output laser beam and the detector field of view were going through its side in accordance with the idea presented in Fig. 10. The correction lens was fabricated using standard glass grinding and polishing method and additionally covered with AR layers. The picture of the assembled setup is presented in Fig. 19.

During the measurements, the target plate was positioned in varying distances z_i (which were measured precisely by a COTS rangefinder), and the detector output voltage V was noted for every z_i. The voltage was proportional to the optical echo power signal, so the vector $V_i = V(z_i)$ represented the function $P(z)$. The measurements were performed for pure LRF, then LRF covered with a dome, and finally – for the corrected system (LRF + dome + correcting lens). Having $P(z)$ measured for all three variants mentioned above, the corresponding geometrical form factor functions were determined. The results are shown in Fig. 20.

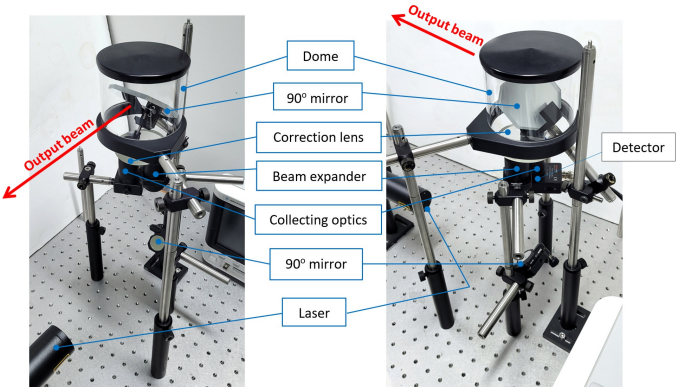

Fig. 19. The picture of the experimental setup

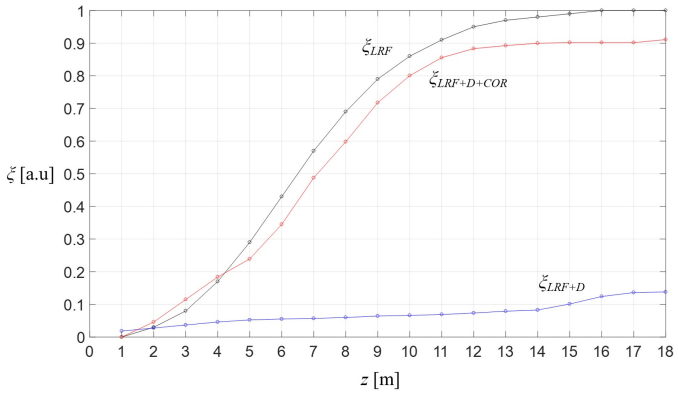

Fig. 20. Results of experimental measurements – geometrical form factors for LRF (black curve), LRF operating from inside the dome (blue curve), and LRF operating from inside the dome; however, equipped with the correcting lens (red curve)

The obtained geometrical form factors show a high agreement with both theoretical expectations and numerical modelling performed in Optic Studio. The application of the glass dome largely devastated the geometrical form factor of the LRF, leading to unsatisfactory performance: $\xi_{\mathrm{LRF+D}} \ll \xi_{\mathrm{LRF}}$. The correction lens allowed the elimination of this problem and resulted in the recovery of the original geometrical form factor: $\xi_{\mathrm{LRF+D+COR}} \approx \xi_{\mathrm{LRF}}$. The observed $\xi_{\mathrm{LRF+D+COR}}(z)$ curve does not reach the value of one, because the applied glass dome was not covered with AR layers. Nevertheless, the experiment proved the efficiency of the proposed correcting method.

Apart from the quantitative analysis discussed above, during the experiments also visual assessment of the laser beam irradiance spatial distribution on the target plate was systematically made. It can be concluded that the observed geometries were similar to those obtained in numerical studies. The laser beam in the "LRF + dome" configuration showed significant aberrations if compared to the pure Gaussian beam of the "pure LRF" configuration. Also, the application of the correcting lens did not eliminate the aberrations; however, it significantly reduced them. For this reason, although the proposed methodology of glass dome impact correction works efficiently in the case of LRF setups, it cannot be applied directly to imaging systems.

For such systems, the correction lens would certainly have to become more complex in shape (aspheric or even freeform). Such analysis is going to be done in the future work.

5. CONCLUSIONS

This paper describes in detail the simple optical correction method dedicated to eliminating the impact of a cylindrical glass dome on laser scanner or laser rangefinder performance. Currently, most laser scanning solutions avoid using this kind of cover due to significant deterioration of the parameters (range, resolution). Instead, more complicated and costly dome types are used.

The proposed approach allows one to use a cylindrical dome, albeit with a correcting plano-cylindrical lens. Such a lens must be positioned in front of the LRF transmitter and receiver in such a way that it is common for both these apertures. The vertex of the correcting lens must be placed exactly at the geometric centre between the optical axis of the transmitter and the receiver. The required radius of curvature of the discussed correcting lens depends on dome parameters (thickness, curvature, refractive index) and LRF itself (laser wavelength, separation between transmitter and receiver, laser beam divergence).

The design method of the correcting lens, numerical modelling of its curing effect on LRF working from inside a cylindrical dome, and finally the experimental results are discussed in the paper. The proposed approach seems to meet the requirements. Its effectiveness was assessed by comparing geometrical form factors of pure LRF vs. LRF operating through a dome and correcting lens. The comparison was based on both numerical modelling and experiments. Both verification methods produced satisfactory results. The application of the designed correcting lens allowed us to restore the original performance of the LRF module, despite it working through a cylindrical dome.

ACKNOWLEDGEMENTS

This work was supported by the European Regional Development Fund under Priority Axis I "Use of research and development activities in the economy" – Action 1.2 "Research and development activities of enterprises" of the Regional Operational Program of the Mazowieckie Voivodeship: Project No. RPMA.01.02.00-14-B498/18 "Laser scanner using a fiber laser", Project No. RPMA.01.02.00-14-B503/18 "Development of a mobile measurement platform using the JAG6 laser together with road object classifiers for image recognition".

REFERENCES

[1] A.P. Spring, "A History of Laser Scanning Part 1: Space and Defense Applications," *Photogramm. Eng. Remote Sens.*, vol. 86, no. 7, pp. 419–429, 2020, doi: 10.14358/PERS.86.7.1.

[2] A.P. Spring,, "A History of Laser Scanning Part 2: The Later Phase of Industrial and Heritage Applications," *Photogramm. Eng. Remote Sens.*, vol. 86, no. 8, pp. 479–501, 2020, doi: 10.14358/PERS.86.8.479.

[3] Y. Zhao, X. Yu, Z. Xin, M. Fan, and H. Wu, "Application and outlook of terrestrial 3D laser scanning technology in forestry," *World For. Res.*, vol. 23, no. 4, pp. 41–45, 2010, doi: 10.3390/s22010265.

[4] M. Javaid, A. Haleem, R.P. Singh, and R. Suman, " Industrial perspectives of 3D scanning: Features, roles and it's analytical applications," *Sensors Int.*, vol. 21, p. 100114, 2021, doi: 10.1016/j.sintl.2021.100114.

[5] I.M. Oludare and B. Pradhan, " A decade of modern cave surveying with terrestrial laser scanning: a review of sensors, method and application development," *Int. J. Speleol.*, vol. 45, no. 1, pp. 71–88, 2016, doi: 10.5038/1827-806X.45.1.1923.

[6] A. Szymczak-Graczyk, Z. Walczak, B. Ksit, and Z. Szyguła, "Multi-criteria diagnostics of historic buildings with the use of 3D laser scanning (a case study)," *Bull. Pol. Acad. Sci. Tech. Sci.*, vol. 70, no. 2, p. e140373, 2022, doi: 10.24425/bpasts.2022.140373.

[7] Z. Mierczyk, Lasers in the dual use technologies,, *Bull. Pol. Acad. Sci. Tech. Sci.*, vol. 60, no. 4, pp. 691–696, 2012, doi: 10.2478/v10175-012-0080-z.

[8] A. Kus, "Implementation of 3D optical scanning technology for automotive applications," *Sensors*, vol. 9, no. 3, pp. 1967–1979, 2009, doi: 10.3390%2Fs90301967.

[9] J. Hoła, J. Bień, Ł. Sadowski, and K. Schabowicz, "Non-destructive and semi-destructive diagnostics of concrete structures in assessment of their durability," *Bull. Pol. Acad. Sci. Tech. Sci.*, vol. 63, no. 1, pp. 87–96, 2015, doi: 10.1515/bpasts-2015-0010.

[10] T. Reyno, C. Marsden, and D. Wowk, " Surface damage evaluation of honeycomb sandwich aircraft panels using 3D scanning technology," *NDT E Int.*, vol. 97, pp. 11–19, 2018, doi: 10.1016/j.ndteint.2018.03.007.

[11] G. Aslan, E.I. Konukseven, A. and B. Koku, " Design and implementation of a 3D scanning platform for mobile robotic applications," *Int. J. Des. Eng.*, vol. 5, no. 4, pp. 358–373, 2015, doi: .

[12] M.M. Jadhav, Y. Durgude, and V.N. Umaje,, "Design and development for generation of real object virtual 3D model using laser scanning technology," *Int. J. Intell. Mechatron. Robot.*, vol. 1, no. 3, pp. 273–291, 2019, doi: 10.1504/IJIMR.2019.101770.

[13] Z. Liu, J. Zhu, L. Yang, H. Liu, J. Wu, and B. Xue, " A single-station multi-tasking 3D coordinate measurement method for large-scale metrology based on rotary-laser scanning," *Meas. Sci. Technol.*, vol 24, p. 105004, 2013, doi: 10.1088/0957-0233/24/10/105004.

[14] L. Pinpin, Q. Wenge, C. Yunjian, and L. Feng, " Application of 3D Laser Scanning in Underground Station Cavity Clusters," *Adv. Civ. Eng.*, vol. 2021, p. 8896363, 2021, doi: 10.1155/2021/8896363.

[15] H. Yuan, H. Zhang, B. Zha, and L. Ding, " Trajectory correction and position error analysis of underwater laser scanning," *Opt. Laser Technol.*, vol. 153, p. 108136, 2022, doi: 10.1016/j.optlastec.2022.108136.

[16] M. Javaid, A. Haleem, S. Khan, and S. Luthra, " Different flexibilities of 3D scanners and their impact on distinctive applications: An analysis," *Int. J. Business Anal.*, vol. 7, no. 1, pp. 37–53, 2020, doi: 10.4018/IJBAN.2020010103.

[17] M. Choi, M. Kim, G. Kim, S. Kim, S.C. Park, and S. Lee, " 3D scanning technique for obtaining road surface and its applications," *Int. J. Precis. Eng. Manuf.*, vol. 18, pp. 367–373, 2017, doi: 10.1007/s12541-017-0044-1.

[18] B.V. Farahani, F. Barros, M.A. Popescu, P.J. Sousa, P.J. Tavares, and P. Moreira, " Geometry acquisition and 3D modelling of a wind tower using a 3D laser scanning technology," *Procedia Struct. Integr.*, vol. 17, pp. 712–717, 2019, doi: 10.1016/j.prostr.2019.08.095.

[19] Y. Chen and D.T. Griffith,, "Experimental and numerical full-field displacement and strain characterization of wind turbine blade using a 3D Scanning Laser Doppler Vibrometer," *Opt. Laser Technol.*, vol. 158, p. 108869, 2023, doi: 10.1016/j.optlastec.2022.108869.

[20] K. Panjvani, A.V. Dinh and K.A. Wahid,, "LiDARPheno – A low-cost lidar-based 3D scanning system for leaf morphological trait extraction," *Front. Plant Sci.*, vol. 10, art. 147, 2019, doi: 10.3389/fpls.2019.00147.

[21] T. Zogheib *et al.*,, "Comparison of 3D Scanning Versus 2D Photography for the Identification of Facial Soft-Tissue Landmarks," *Open Dent. J.*, vol. 12, pp. 61–71, 2018, doi: 10.2174/1874210601812010061.

[22] J.F. Larue, D. Brown, and M. Viala, "How optical CMMs and 3D scanning will revolutionise the 3D metrology world," in *Integrated Imaging and Vision Techniques for Industrial Inspection*, ed. Z. Liu, H. Ukida, P. Ramuhalli, K. Niel, Springer, 2015, pp. 141–176.

[23] D. Moon, S. Chung, S. Kwon, J. Seo, and J. Shin, " Comparison and utilisation of point cloud generated from photogrammetry and laser scanning: 3D world model for smart heavy equipment planning," *Autom. Constr.*, vol. 98, pp. 322–331, 2019, doi: 10.1016/j.autcon.2018.07.020.

[24] B. Ergun, "A novel 3D geometric object filtering function for application in indoor area with terrestrial laser scanning data," *Opt. Laser Technol.*, vol. 42, no. 5, pp. 799–804, 2010, doi: 10.1016/j.optlastec.2009.12.006.

[25] B.V. Farahani *et al.*, "A coupled 3D laser scanning and digital image correlation system for geometry acquisition and deformation monitoring of a railway tunnel," *Tunn. Undergr. Space Technol.*, vol. 91, p. 102995, 2019, doi: 10.1016/J.TUST.2019.102995.

[26] M.C. Amann, T.M. Bosch, M. Lescure, R.A. Myllylae, and M. Rioux, "Laser ranging: A critical review of usual techniques for distance measurement," *Opt. Eng.*, vol. 40, no. 1, pp. 10–19, 2001, doi: 10.1117/1.1330700.

[27] E. Hecht, *Optics*, fourth ed., San Francisco, Addison Wesley, 2002.

[28] J. Wojtanowski, M. Zygmunt, M. Traczyk, Z. Mierczyk, and M. Jakubaszek, "Beam forming optic aberrations' impact on maximum range of semiconductor laser based rangefinders," *Opto-Electron. Rev.*, vol. 9, no. 3, pp. 152–161, 2014, doi: 10.2478/s11772-014-0191-1.

[29] R.M. Measures, *Laser Remote Sensing Fundamentals and Applications*, reprint ed., Malabar, Krieger Publishing Company, 1992.

[30] J. Wojtanowski,, "Cancelling lidar echo signal 1/range^2 dependence and geometrical form factor shaping by the application of freeform optics," *Opt. Laser Technol.*, vol. 125, p. 106011, 2020, doi: 10.1016/j.optlastec.2019.106011.

[31] W. Smith, *Modern Optical Engineering*, fourth ed., New York, Mc Graw Hill, 2008.